Nonlinear Dynamics manuscript No.
(will be inserted by the editor)

Nonlinear analysis, instability and routes to chaos of a cracked rotating shaft

Saber El Arem

Received: date / Accepted: date

Abstract The aim of this paper is to explore the dynamical response of a rotating shaft with a cracked transverse section. This complex problem is distilled down to the study of a very comprehensive mechanical system composed of two non-cracked rigid bars connected with a nonlinear bending spring that concentrates the global stiffness of the cracked shaft. The switching crack model is presented as a specific case of the EDF-LMS family of models and adopted to describe the breathing mechanism of the crack. By analyzing the system equilibrium equations, we show that the stiffness change when the crack breathes leads to shocks with velocity jumps and coupling between the transverse oscillations. The linear stability of the periodic solutions is examined based on the Floquet's theory. Nonlinear dynamics tools such as Poincaré maps and bifurcation diagrams are used to unveil the system oscillations characteristics. Many well-known features due to the crack presence have been observed, but some unexpected responses are noticed like chaotic behavior. This can be confidently attributed to the abrupt change of the structure stiffness with the breathing crack. It has also been observed that with the super-harmonic resonance phenomenon, the increase of static deflection accompanied by that of the first two harmonics amplitudes are good indicators of a propagating crack presence.

Keywords Rotating shaft · breathing crack · Shocks · nonlinear dynamics · stability · Floquet's theory · routes to chaos · bifurcation diagram · Poincaré section

S. El Arem
Arts et Métiers ParisTech
Laboratoire LAMPA, CER Angers, France
E-mail: saber.elarem@ensam.eu

Nomenclature

Symbol	Description
t	time
AG, GB	Rigid bars connected at G: non-cracked parts of the shaft
G	Center of cracked transverse section
a, b	Rigid bars lengths
D	Viscous damping coefficient
d	Reduced (dimensionless) viscous damping coefficient
H_0	Assumption of small motions near the equilibrium position
H_1	Assumption a step function to describe the breathing mechanism of the crack
U, V	Displacements of G
θ_x, θ_y	Rotation angles about (Ox) and (Oy)
(Oxy)	The inertial non-rotating frame
$(G\zeta\eta)$	The body-fixed rotating frame
W_s^*	Total elastic energy of the non-cracked shaft
W^*	Total elastic energy of the cracked shaft
w^*	Additional (complementary) elastic energy due to the crack
w	Additional elastic energy due to the crack
Φ	Aperture angle
S	Transverse section area
$\mathbf{s}(\Phi)$	System compliance function
$\mathbf{s}'(\Phi)$	Derivative of the system compliance function
$M = (M_x, M_y)$	Bending moments at the cracked transverse section
E	Young modulus
I	Quadratic moment of inertia
$\varphi = \arctan(\frac{[\theta_y]}{[\theta_x]})$	Response angle
$\mathbf{k}(\varphi)$	System stiffness function
$\mathbf{k}'(\varphi)$	Derivative of the system stiffness function
M_0	Diagonal element of the mass matrix
$[\dot{U}]$, $[\dot{V}]$	Velocities jumps
Δ	Measures the system stiffness loss
g	Acceleration of gravity
m	Linear mass density
m_2	System total mass
Ω	Rotating speed
$1X\Omega$	Once per revolution harmonic component
$2X\Omega$	Twice per revolution harmonic component
$nX\Omega$	n-times per revolution harmonic component $(n = 3, 4, \dots)$

1 Introduction

The presence of a crack in an engineering structure introduces a local flexibility that alters its vibratory behavior. It's now understood that this local flexibility is induced

by the strain energy concentration in the vicinity of the crack tip (Irwin [17], Bui [4]). Unless detected in time, propagating cracks could affect seriously the system integrity which could not be tolerated in industries like power plants, aeronautics and aerospace.

Since the early 1970s when investigations on the dynamics of cracked rotors began, numerous papers on this subject have been published [6, 26, 3] and specialists from industry and academia agree on the fact that the modeling and analysis of the behavior of cracked rotating shafts are complex. Moreover, to build a reliable model, a special feature inherent to this problem has to be considered meticulously: the crack breathing mechanism as presented in Fig.1. In fact, when the structure rotates, the crack opens and closes depending on the stresses at the crack surface. This mechanism is at the origin of the nonlinear aspect of the problem. During the last three

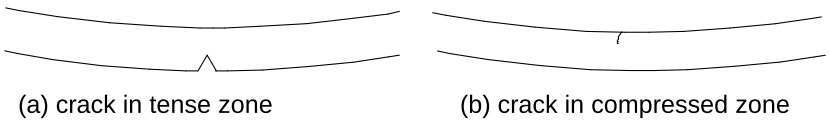

Fig. 1 *Crack breathing mechanism*

decades, great attention has been paid by several research scientists to the analysis and diagnosis of cracks in rotating machinery. The most relevant experimental and numerical works related to cracked structures modeling could be found in some review articles [6, 31, 14] and books [3, 7].

In this article, we continue to advance a family of models and discussions we have started developing nearly twenty years ago at Electricité De France (EDF) and the Solid Mechanics Laboratory (LMS) of École Polytechnique in France. All these models belong to what we have called the EDF−LMS approach as described in [10]. It provides means to overcome the difficulties and imprecisions ([25, 5]) inherent to the first and oldest approach initiated in the 1970s by Dimarogonas and his coworkers and based on the linear fracture mechanics principles [26].

1.1 A brief review of the EDF−LMS approach

The key idea of the EDF−LMS approach, as described in many articles (Andrieux and Varé [2], El Arem [9]), is the identification of the characteristics of a beam-like model (Fig.2(c)) from accurate three-dimensional (3D) finite element model, cf. Fig.2(a). With the large number of capabilities offered by the 3D modeling, it becomes possible to consider cracks of complex shapes and various loading conditions which makes the approach generic and its application to similar problems straightforward.
In the beam-like model, the cracked transverse section (Fig.2(b)) is replaced by a

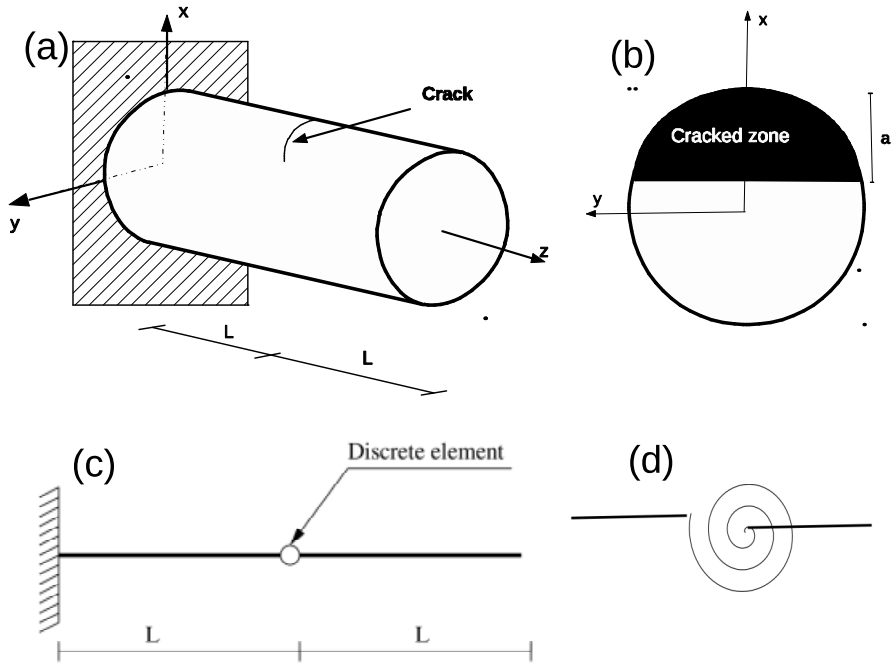

Fig. 2 *The cracked shaft model of [2]*

lumped (zero length) nonlinear bending spring (Fig.2(d)) whose constitutive equations give a complete description of the crack breathing mechanism. It was demonstrated by El Arem [9] that the shearing effects on the breathing mechanism of the crack are negligible and, thus, will not be considered in what follows.
The cracked 3D structural element of Fig.2(a) is subjected to an end moment $M_{2L} = (M_x(2L), M_y(2L))$ at $z = 2L$. The energy function could be written by distinguishing the contribution of the cracked transverse section from that of the non-cracked parts, in the form:

$$W^*(M_{2L}) = W^*(M) = W_s^*(M) + w^*(M) = \frac{L}{EI}||M||^2(1+\mathbf{s}(\Phi)) \qquad (1)$$

where $M = (M_x, M_y)$ is the resulting couple of bending moments at the cracked section, W_s^* the total elastic energy of non-cracked (healthy) structure subjected to the bending moment M and w^* the additional elastic energy due to the presence of the cracked section. In order to simulate a rotating load on a fixed beam, the bending load is applied in several aperture angles $\Phi = \arctan(\frac{M_y}{M_x})$, with Φ varying over $[0, 2\pi[$. E is the Young modulus and I quadratic moment of inertia.
In this framework, the nonlinear constitutive equations of the discreet element modeling the cracked transverse section are obtained by derivation of the function w^* with

respect to M. We obtain

$$[\theta] = \begin{pmatrix} [\theta_x] \\ [\theta_y] \end{pmatrix} = \frac{2L}{EI} \begin{pmatrix} \mathbf{s}(\Phi) & -\frac{1}{2}\mathbf{s}'(\Phi) \\ \frac{1}{2}\mathbf{s}'(\Phi) & \mathbf{s}(\Phi) \end{pmatrix} \begin{pmatrix} M_x \\ M_y \end{pmatrix}, \text{with } \mathbf{s}'(\Phi) = \frac{d\mathbf{s}(\Phi)}{d\Phi} \tag{2}$$

However, for finite element computational codes in rotor dynamics, a nonlinear relation of the form $[\theta] = f(M)$ is to be identified. Thus, the identification process was formulated in terms of the additional deformation energy $w([\theta])$ written as a quadratic function of the rotations jumps at the cracked transverse section:

$$w([\theta_x],[\theta_y]) = \frac{EI}{4L}\mathbf{k}(\varphi)|||[\theta]|||^2 \text{ with } \varphi = \arctan(\frac{[\theta_y]}{[\theta_x]}) \tag{3}$$

The function $\mathbf{k}$ describes the system stiffness variation with the crack breathing. It is deduced from the compliance function $\mathbf{s}$ that was identified using 3D numerical simulations. The relation between $\mathbf{k}$ and $\mathbf{s}$ is established by the Légendre-Fenchel transform relating w to w^* as detailed in [2, 8, 9].
The constitutive equations are obtained by differentiating w with respect to $[\theta]$ as:

$$\begin{pmatrix} M_x \\ M_y \end{pmatrix} = \frac{EI}{2L} \begin{pmatrix} \mathbf{k}(\varphi) & -\frac{1}{2}\mathbf{k}'(\varphi) \\ \frac{1}{2}\mathbf{k}'(\varphi) & \mathbf{k}(\varphi) \end{pmatrix} \begin{pmatrix} [\theta_x] \\ [\theta_y] \end{pmatrix} \text{ with } \mathbf{k}'(\varphi) = \frac{d\mathbf{k}(\varphi)}{d\varphi} \tag{4}$$

For straight tip cracks, the crack is totally closed when $\varphi \in [0,\pi[$ and

$$\begin{cases} \mathbf{k}(\varphi) = +\infty \\ \mathbf{k}'(\varphi) = 0 \end{cases} \tag{5}$$

For $\varphi \in [\pi, 2\pi[$, the crack is partially open (closed). It opens totally (lowest stiffness) at $\varphi = \frac{3\pi}{2}$. This approach was first presented by Andrieux and Varé [2] and experimentally validated by Stoisser and Audebert [30] then largely discussed and improved in [8, 12, 9]. This variation of the stiffness of the nodal element representing the cracked transverse section will be, in the next part of this paper, adapted to be used in a two-Degrees-Of-Freedom (2−DOF) dynamical system describing a rotating shaft with a cracked transverse section.

1.2 Nonlinear analysis of a cracked rotating shaft

In analyzing the dynamics of cracked rotating shafts, it is often assumed that the vibration induced stresses are small compared to those due to static loads which is commonly accepted for horizontal heavy rotors of industrial plants. With this hypothesis, the system global stiffness variation becomes depending only on the angular position Ωt of the crack with respect to the inertial (non-rotating) frame. Consequently, the obtained differential equations describing the dynamical equilibrium of the system are linear with periodic coefficients ([21, 19, 14]). However, as detailed by Bachschmid et al [3], in many situations like :

– lightweight rotors and lightly damped rotors when passing a critical rotating frequency

- vertical axis rotors where the static bending moments are small
- a crack that has developed in a rotor transverse section where the bending moments are small

the breathing mechanism becomes dependent not only but significantly on the dynamical response of the system. Thus, we have systematically integrated this nonlinear dependence in the formulation of the EDF−LMS approach to make it capable of handling different situations of cracking in rotating machines.
Nonlinear aspects of cracked rotating shafts have recently interested many researchers [20, 1]. In fact, these very expensive structures are omnipresent in sectors like aeronautics, aerospace, and power generation where loading conditions and environment are prone to cracking. An overview of the most observed phenomena when examining the response of a cracked rotor could be found in [18] where harmonic, superharmonic, subharmonic and simultaneous sub/super harmonic resonances are well commented and explained using a simple rotor model similar to Jeffcott rotor. By considering a switching crack model, Patel and Darpe [27] observed chaotic and quasi-periodic dynamical responses. The authors examined the effect of the unbalance eccentricity level, the crack depth and damping on the bifurcation characteristics of a cracked rotor. It was reported that with a more realistic breathing mechanism of the crack, the chaotic, quasi-periodic and subharmonic vibrations are not observed on the response of the cracked rotor for the similar set of parameters. Similar conclusions where formulated in [13] where the authors have found that with a smooth stiffness variation when the crack breathes, the cracked shaft never exhibits chaotic or quasi-periodic vibratory response. Also, Muller et al [23] observed chaotic motions and strange attractors by applying the theory of Lyapunov exponents to a system with the switching crack model of Gasch [14].

1.3 Aim and plan of the article

In this article, we focus mainly on the crack presence effects on the dynamical response of the shaft, hence the problem is distilled down to its essential aspects: the equilibrium equations are written in a simple, comprehensive and uncluttered form. In section 2, we give a detailed description of the cracked shaft model and establish the equilibrium equations of the system. When a simplifying assumption is utilized, the breathing mechanism becomes dependent only on the angular position of the crack Ωt and linear equilibrium equations are obtained. In section 3, we use the harmonic balance method to solve the system of linear equations. We show that with a switching crack model, the abrupt opening/closing of the crack generates shocks with velocity jumps responsible for coupling between the system transverse oscillations. The first part of Section 4 is devoted to stability analysis of the periodic solutions based on Floquet's theory. In the second part, we examine meticulously, using the bifurcation diagrams and Poincaré sections, three zones of instability to characterize their corresponding phenomena. In section 5, we give some conclusions and perspectives to help in crack signature identification in rotating shafts.

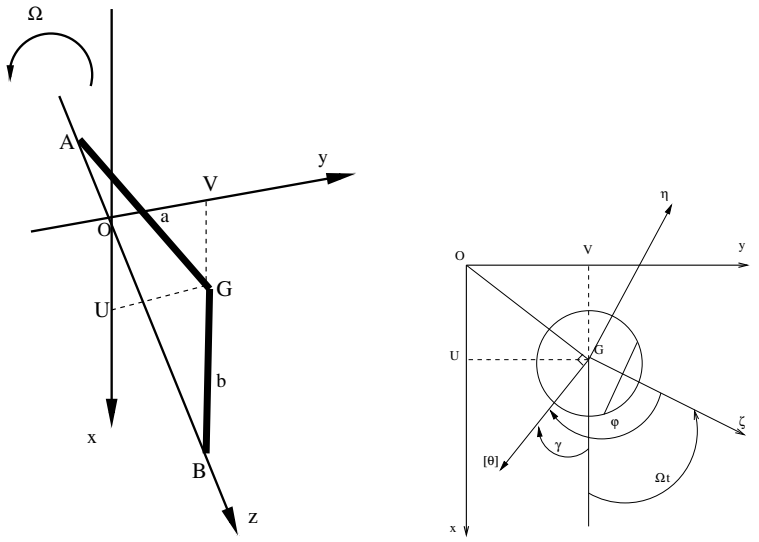

(a) Mechanical system (b) Cracked transverse section

Fig. 3 *Mechanical system. (Oxy) inertial frame and (Gζη) rotating frame*

2 The cracked shaft description and parameters

The mechanical system modeling the cracked rotating shaft (Fig.3) is composed of two non-cracked rigid bars AG and GB of circular section S, of respective lengths a and b, and distributed mass m. They are connected, in G, by a nonlinear elastic bending spring that represents the global stiffness of the cracked shaft. The system is simply supported at A and B, rotating at the frequency Ω about the bars axis and subjected to the effects of its own weight.
In what follows, we assume small motions near the equilibrium position under the shaft's own weight (assumption H_0).
In the inertial frame, the small movements of G are described by $(U(t),V(t),0)$.
Let $M(x,y,z)$ be a point (transverse section) of the rotating system. Its coordinates x, y and z in the inertial frame are given by:

$$\begin{cases} (x=\frac{z+a}{a}U, y=\frac{z+a}{a}V, z) \text{ if } M\in[GA] \\ (x=\frac{b-z}{b}U, y=\frac{b-z}{b}V, z) \text{ if } M\in[GB] \end{cases} \tag{6}$$

The respective rotation angles about (Ox) and (Oy) are:

$$\theta_x=-\frac{\partial y}{\partial z}=\begin{cases} -\frac{V}{a} \text{ if } M\in[GA] \\ \frac{V}{b} \text{ if } M\in[GB] \end{cases} \text{ and } \theta_y=\frac{\partial x}{\partial z}=\begin{cases} \frac{U}{a} \text{ if } M\in[GA] \\ -\frac{U}{b} \text{ if } M\in[GB] \end{cases} \tag{7}$$

Under the H_0 assumption, the rotations gaps in G could be written as:

$$[\theta] = \begin{cases} [\theta]_x \\ [\theta]_y \end{cases} = \begin{cases} \theta_x(0^+) - \theta_x(0^-) = (\frac{1}{a} + \frac{1}{b})V \\ \theta_y(0^+) - \theta_y(0^-) = -(\frac{1}{a} + \frac{1}{b})U \end{cases}$$

We can notice in particular that: $[\theta] \perp OG$.
The crack orientation is defined by the $G\zeta$ direction given by: $(Ox, G\zeta) = \Omega t$.

The elastic energy of the system could be written as quadratic form of the rotations gaps:

$$W([\theta]_x, [\theta]_y) = \frac{1}{2}\mathbf{k}(\varphi)([\theta]_x^2 + [\theta]_y^2) \tag{8}$$

where $\mathbf{k}(\varphi)$ represents a directional stiffness, 2π-periodic function of the angle

$$\varphi = (G\zeta, [\theta]) = (G\zeta, Ox) + (Ox, [\theta]) = -\Omega t + \gamma \in [0, 2\pi[\ modulo \ 2\pi$$

where γ is given by $\gamma = -\arctan(\frac{U}{V}) + n\pi$, with $n \in \{0, 1, 2\}$, cf. Fig.3.
The bending moments associated with the rotations at time t are:

$$M_x = \frac{\partial W}{\partial [\theta]_x} \text{ and } M_y = \frac{\partial W}{\partial [\theta]_y}$$

In the rotating shaft fixed frame $(G\zeta\eta)$, the following constitutive equations are then obtained as proposed in [2, 8]:

$$\begin{pmatrix} M_\zeta \\ M_\eta \end{pmatrix} = \begin{pmatrix} \mathbf{k}(\varphi) & -\frac{1}{2}\mathbf{k}'(\varphi) \\ \frac{1}{2}\mathbf{k}'(\varphi) & \mathbf{k}(\varphi) \end{pmatrix} \begin{pmatrix} [\theta]_\zeta \\ [\theta]_\eta \end{pmatrix} \tag{9}$$

This nonlinear relation is written

$$\begin{pmatrix} M_x \\ M_y \end{pmatrix} = \begin{pmatrix} \mathbf{k}(\varphi) & -\frac{1}{2}\mathbf{k}'(\varphi) \\ \frac{1}{2}\mathbf{k}'(\varphi) & \mathbf{k}(\varphi) \end{pmatrix} \begin{pmatrix} [\theta]_x \\ [\theta]_y \end{pmatrix} \tag{10}$$

in the inertial non-rotating frame (Oxy).
By writing the constitutive equations of the cracked section in this form we concentrate the breathing mechanism of the crack in one single parameter: $\mathbf{k}(\varphi)$. Also, we should highlight the fact that the stiffness loss in both directions ($G\zeta$ and $G\eta$) are taken into consideration since it is well known that the stiffness also reduces along the stronger axis ($G\eta$) as the crack propagates [19]. This aspect was neglected by Gasch [14] where only stiffness reduction in the weak direction of the crack ($G\zeta$) is considered.
The dynamical equilibrium equations are given by the Virtual Powers Principle as:

$$\begin{cases} M_0\ddot{U}(t) + D\dot{U}(t) + \mathbf{k}(\varphi)U(t) - \frac{1}{2}\mathbf{k}'(\varphi)V(t) = m_2 g \\ M_0\ddot{V}(t) + D\dot{V}(t) + \mathbf{k}(\varphi)V(t) + \frac{1}{2}\mathbf{k}'(\varphi)U(t) = 0 \end{cases} \tag{11}$$

where $M_0 = \frac{\rho S}{3}(a+b)\mathfrak{L}^2 + \rho I\mathfrak{L}, m_2 = m\frac{a+b}{2}\mathfrak{L}^2$ and $\frac{1}{\mathfrak{L}} = \frac{1}{a} + \frac{1}{b}$, $D = 2dM_0w_0$ is the viscous damping coefficient, d the reduced (dimensionless) damping coefficient

and $w_0 = \sqrt{\frac{K_0}{M_0}}$ the natural frequency of the system with the global stiffness K_0.
Under the H_0 assumption, we have:

$$|U| \gg V$$

Consequently, γ is close to $\frac{3\pi}{2}$ so that the approximation

$$\varphi = \frac{3\pi}{2} - \Omega t \tag{12}$$

is justified and it becomes possible to solve system (11) using the harmonic balance method.
In the next section, the following assumptions will be adopted:

1. H_0: small motions near the equilibrium position under the shaft's own weight,
2. H_1: a step function to describe the breathing mechanism of the crack.

The harmonic balance method will be utilized to solve the equilibrium equations.

3 Harmonic balance: Periodic solutions under H_0 and H_1 assumptions

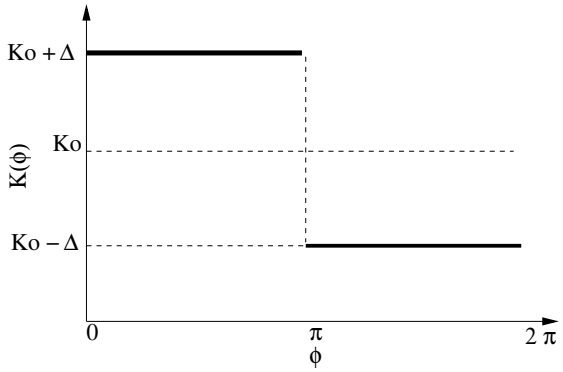

Fig. 4 *Periodic global stiffness function: switching crack model*

The global stiffness of the system is described by the periodic step function (Fig.4)

$$\mathbf{k}(\varphi) = \begin{cases} K_0 + \Delta & \forall \ \varphi \in [0, \pi[\\ K_0 - \Delta & \forall \varphi \ \in [\pi, 2\pi[\end{cases} \tag{13}$$

Thus, the crack is totally closed for $\varphi \in [0, \pi[$, and totally open for $\varphi \in [\pi, 2\pi[$. The difference with the model presented by El Arem and Nguyen [13] is that the current model does not consider the partial opening/closing of the crack for $\varphi \in [\pi, 2\pi[$.
The global stiffness of the cracked shaft is concentrated at the nonlinear spring. With this representation:

1. the phenomenon of crack closure is taken into account in an exact way by setting the system global stiffness to its value for a non-cracked shaft,
2. the resort to the penalization technique when the crack closes totally is avoided and the numerical simulations cost is reduced by 20 to 100 times as noticed by El Arem and Maitournam [12].

When the shaft rotates, its global stiffness switches from $\mathbf{k}(\varphi) = K_s = K_0 + \Delta$ (fully closed crack) to $\mathbf{k}(\varphi) = K_0 - \Delta$ (fully opened crack). K_s is the global stiffness of the non-cracked shaft.
It is important to notice that only one measurement is required to identify the stiffness function $\mathbf{k}(\varphi)$. In fact, knowing the mass M_0 and the first critical frequency $w_s = \sqrt{\frac{K_s}{M_0}}$ of the non-cracked shaft, we need only to measure the current critical frequency $w_0 = \sqrt{\frac{K_0}{M_0}}$ of the rotating shaft to identify the loss of global stiffness Δ by $\Delta = K_s - K_0$.

When $\varphi \neq n\pi, n \in Z$, we obtain two uncoupled oscillators described by:

$$\begin{cases} M_0\ddot{U}(t) + D\dot{U}(t) + \mathbf{k}(\varphi)U(t) = p_0 \\ M_0\ddot{V}(t) + D\dot{V}(t) + \mathbf{k}(\varphi)V(t) = 0 \\ \mathbf{k}(\varphi) = K_0 + \Delta, \quad \forall\ t/2n\pi < \frac{3\pi}{2} - \Omega t < (2n+1)\pi, n \in Z \\ \mathbf{k}(\varphi) = K_0 - \Delta, \quad \forall\ t/(2n+1)\pi < \frac{3\pi}{2} - \Omega t < (2n+2)\pi, n \in Z \end{cases} \tag{14}$$

At each stiffness change ($\varphi = n\pi, n \in Z$), a shock happens. It corresponds to a sudden acceleration due to interior force of impulse type leading to velocity jumps $[\dot{U}] = \dot{U}_+ - \dot{U}_-$ and $[\dot{V}] = \dot{V}_+ - \dot{V}_-$. While interpreting (11) in distributions form, we obtain the jumps equations as:

$$\begin{cases} M_0[\dot{U}] - \frac{\Delta}{\Omega}V = 0 \\ M_0[\dot{V}] + \frac{\Delta}{\Omega}U = 0 \\ \forall\ t/\frac{3\pi}{2} - \Omega t = 2n\pi, n \in Z \end{cases} \tag{15}$$

$$\begin{cases} M_0[\dot{U}] + \frac{\Delta}{\Omega}V = 0 \\ M_0[\dot{V}] - \frac{\Delta}{\Omega}U = 0 \\ \forall\ t/\frac{3\pi}{2} - \Omega t = (2n+1)\pi, n \in Z \end{cases} \tag{16}$$

The last three systems of equations completely describe the shaft oscillations. Equations (15) and (16) show that the coupling between the transverse oscillations is due only to the shocks with velocity jumps. At each shock, the system accelerates or decelerates to maintain the imposed rotating frequency Ω. The existence of a periodic solution means that the total energy exchanged over one period is null.
When $\mathbf{k}(\varphi)$ is written as a Fourier series using the approximation (12), one obtains continuous functions and consequently shocks are not considered explicitly. The shaft vibratory response can also be split,

$$U(t) = U_0 + u(t), \qquad V(t) = V_0 + v(t) \tag{17}$$

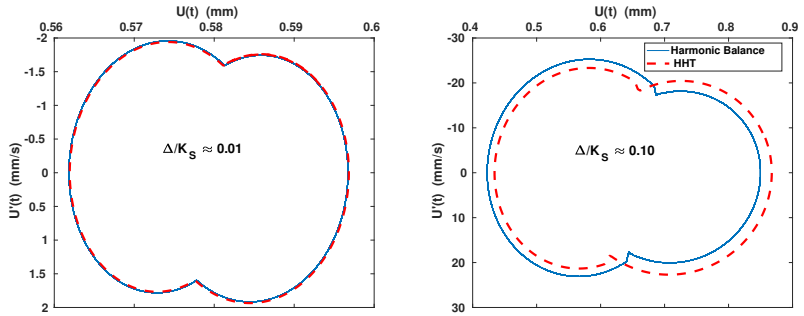

Fig. 5 *Validity of approximation (12), d=0.03,* $\xi = \frac{\Omega}{w_0} = 0.75$

where $(U_0 = \frac{m_2 g}{K_0}, V_0 = 0)$ is the static response of the shaft with the global stiffness K_0 subjected to its own weight.

In the complex plane, the equilibrium equations lead to:

$$M_0\ddot{z}(t) + D\dot{z}(t) + \left(K_0 + \frac{\Delta}{\pi}\sum_{n\in Z}(-1)^n \frac{2n+1}{2n-1} e^{i(2n-1)\Omega t}\right) z(t) = \frac{U_0\Delta}{\pi}\sum_{n\in Z}(-1)^{n+1}\frac{2n+1}{2n-1}e^{i(2n-1)\Omega t} \tag{18}$$

where $z(t) = u(t) + iv(t)$ with $i^2 = -1$. By using the harmonic expansion method, the system response is approximated by

$$z(t) \approx \frac{U_0\Delta}{\pi K_0}\sum_{j=-N}^{j=N} z_j e^{ij\Omega t}$$

and (18) becomes

$$\sum_{j=-N}^{j=N}(1-(j\xi)^2 + 2ijd\xi)z_j e^{ij\Omega t} + \frac{\Delta}{\pi K_0}\sum_{j=-N}^{j=N} z_j \sum_{k=-N}^{k=N}(-1)^k \frac{2k+1}{2k-1} e^{i(2k-1+j)\Omega t} = \sum_{n=-N}^{n=N}(-1)^{n+1}\frac{2n+1}{2n-1}e^{i(2n-1)\Omega t} \tag{19}$$

The problem leads to the determination of a solution of an algebraic system of $(2N+1)$ unknowns, the z_j with $-N \le j \le N$.

The next step is to check the validity of the approximation we have made so far to make the previous developments possible:

$$\varphi = \frac{3\pi}{2} - \Omega t$$

Fig.5 shows a good agreement between the numerical solution of system (11) using

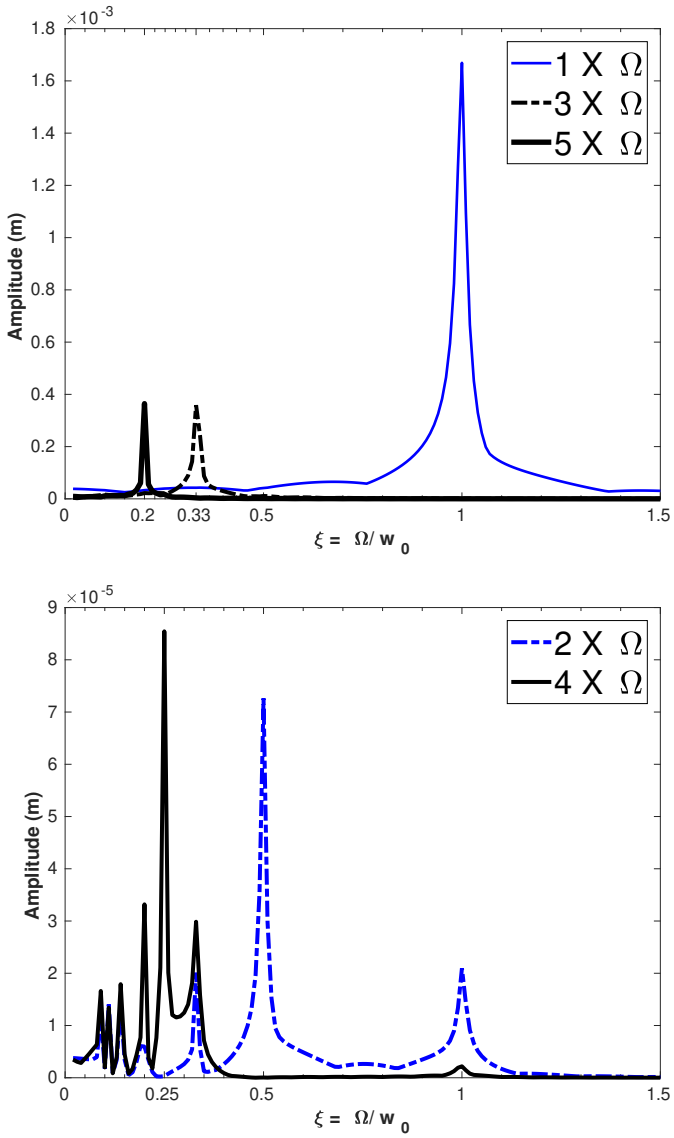

Fig. 6 *Harmonics* $1\times\Omega$ *to* $5\times\Omega$ *amplitudes, d=0.01,* $\frac{A}{K_s}=0.05$

the Hilber-Hughes-Taylor (HHT) α-method ([15]) and that obtained using the harmonic balance method: approximation (12) is consequently justified for small crack depths. For very deep cracks, however, and at the resonance points the shaft displacements are larger and the assumption of small motion (assumption H_0) is not satisfied. Therefore, approximation (12) becomes inadequate: besides the rotation angle of the shaft, the breathing mechanism depends, henceforth, on the vibration amplitude. For

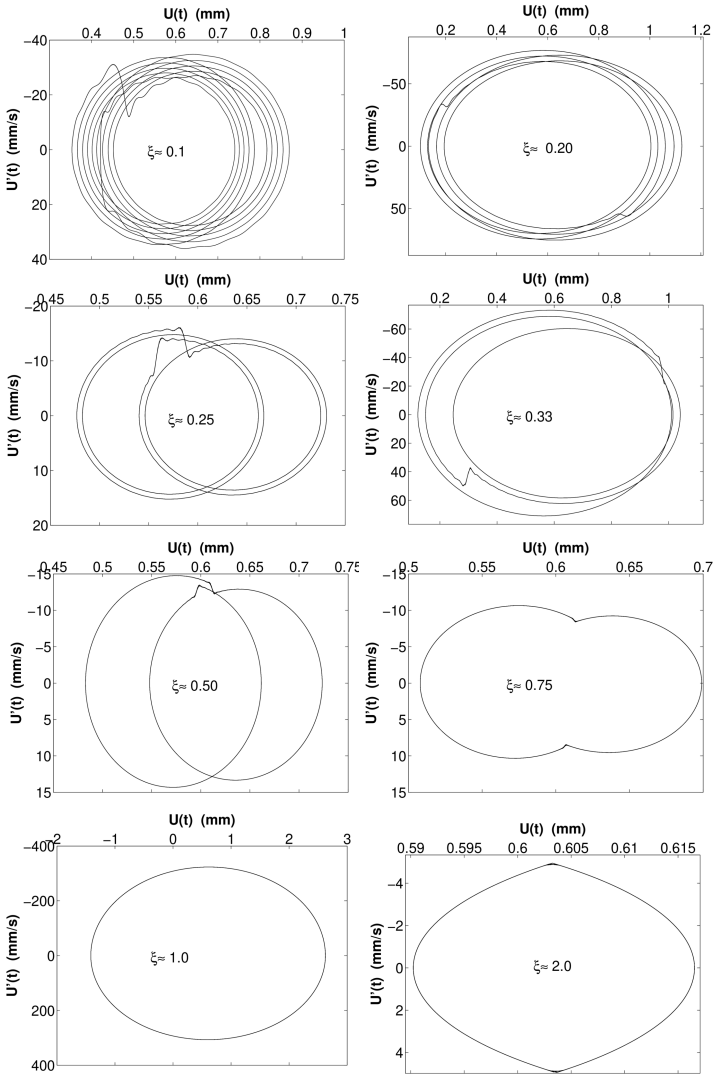

Fig. 7 *Examples of the shaft phase portraits, d=0.01,* $\frac{\Delta}{K_s} = 0.05$

small crack depths, when the shaft is running at sub-multiples of the critical rotating speed ($\xi = \frac{\Omega}{w_0} \approx \frac{1}{N}, N \in \mathbb{N}$), the super-harmonic resonance phenomenon is observed: a resonance peak lies at the frequency $w = N\Omega$ (Fig.6) and the shaft orbit is composed of N loops, cf. Fig.7. This phenomenon, well-known by research scientists dealing with cracked rotors dynamics, was also observed by Gasch [14] and Patel and Darpe [27] by using a switching crack model. This change of the whirl orbit shape during the passage through one-half and one-third of the first critical rotating

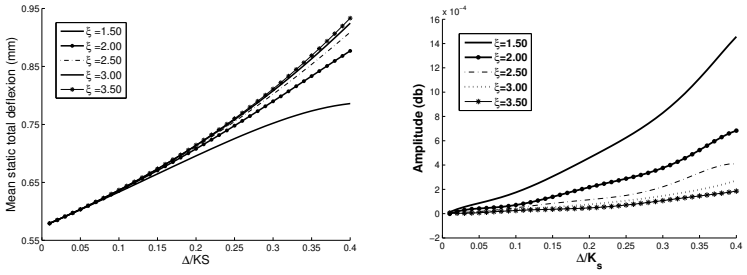

(a) *Static deflection* (b) *First harmonic:* $1 \times \Omega$

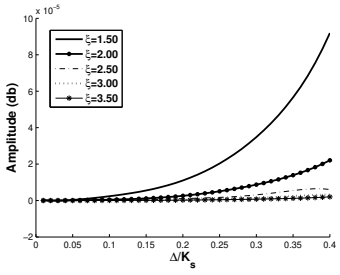

(c) *Second harmonic:* $2 \times \Omega$

Fig. 8 *Static deflection,* $1 \times \Omega$ *and* $2 \times \Omega$ *harmonics amplitude increase with crack depth.*

frequency has been experimentally observed in [32, 29, 16]. Also, in previous works ([11, 13, 12, 8]), we have made similar observation with a more realistic breathing mechanism of the crack.

When looking at the phase diagrams of Fig.7, we can easily notice the velocity jumps at each opening/closing of the crack. These jumps correspond to the abrupt change in the global stiffness of the system.

For supercritical rotating speeds $(\xi \geq 1)$, the system oscillations are dominated by the first harmonic component. Here, the mean total static deflection increases remarkably with the global stiffness loss, but remains less sensitive to the shaft rotating speed variation when $\frac{\Delta}{K_s} < 0.15$. However, for deep cracks, its increase with the rotating frequency becomes measurable, cf. Fig.8(a). The vibration amplitude $(1\times$ and $2\times$ components) increases with the stiffness loss but decreases with the rotation speed, cf. Fig.8(b) and Fig.8(c). Similar conclusions were drawn based on experimental investigations [28] that showed the increase of the $2\times$ and $3\times$ harmonics with the crack depth and noticeable variation of higher-order harmonics components [29, 16, 32] in the subcritical speed zones. Continuous real-time monitoring of these parameters would be of great benefit for propagating cracks detection.

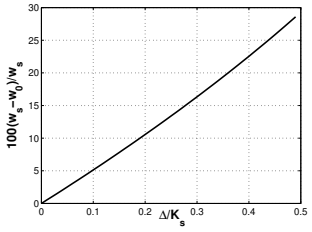

Fig. 9 *Critical frequency drop due to the crack*

According to Dimarogonas [6], the measurement of the change in the first critical speed is not an efficient way to monitor shaft cracks since it is, for small crack depths, proportional to $(\frac{a}{D})^2$. In fact, the author found that an edge crack with depth 54% of the radius produced a 5.6% (overestimated) change in the lowest critical speed of the shaft. Thus, for our model, we can conclude that for $\frac{\Delta}{K_s}$ greater than 20%, the cracks we are dealing with become very deep $(\frac{a}{D} > 50\%)$, cf. Fig.9.

In the next section, we will be conducting a stability analysis based on the Floquet's

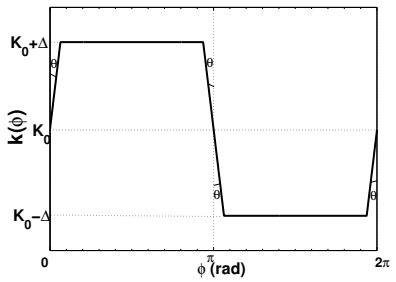

Fig. 10 *Stiffness function k used for the numerical integration of system (11)*

theory. Deep cracks will be considered and, consequently, the HHT numerical scheme will be used instead of the harmonic balance method.

4 Linear stability analysis: Floquet theory

The linear stability of the periodic solutions of system (11) is examined using the Floquet's theory. This method has been intensively used [14, 22, 8, 13] for the stability analysis of cracked rotors and more generally for systems governed by linear ordinary differential equations with periodic coefficients [24]. The simplifying condition (12) will no longer be considered in what follows: the system stiffness is henceforth response-dependent causing the equilibrium equations to be nonlinear. The HHT method is used for the time integration of the system. This direct time-integration method is an elegant way to introduce damping in the Newmark method without degrading the order of accuracy.

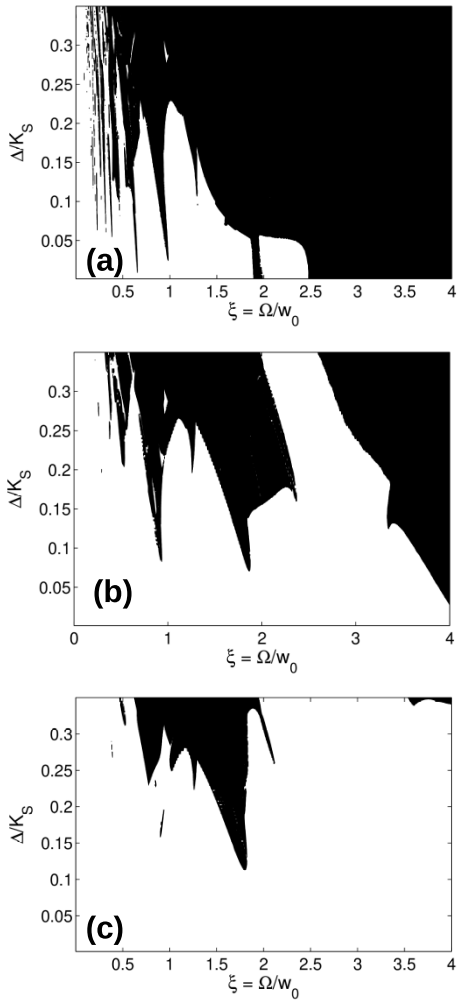

Fig. 11 *Stable and unstable (hatched) zones*. (a): $d = 1\%$, (b): $d = 3\%$, (c): $d = 5\%$.

For the numerical integration of the dynamical equations (11), we have considered an approximation of the stiffness function $\mathbf{k}$ to account for the extra-diagonal terms of the stiffness matrix ($\frac{1}{2}\mathbf{k}'(\varphi)$ and $-\frac{1}{2}\mathbf{k}'(\varphi)$). In this approximation, θ is taken very small ($\tan(\theta) \approx \dfrac{1}{10K_s}$) to ensure sufficient representation of the abrupt change in the system's global stiffness (Fig.10).To ensure the system instability is not due to numerical divergence problem, we have considered very high sampling frequency by dividing the forcing period $\frac{1}{\Omega}$ into 20000 integration steps.
Fig.11 shows the stable and unstable (hatched) zones for three different values of the dissipation coefficient d. Mainly, we distinguish three zones of instabilities: the first

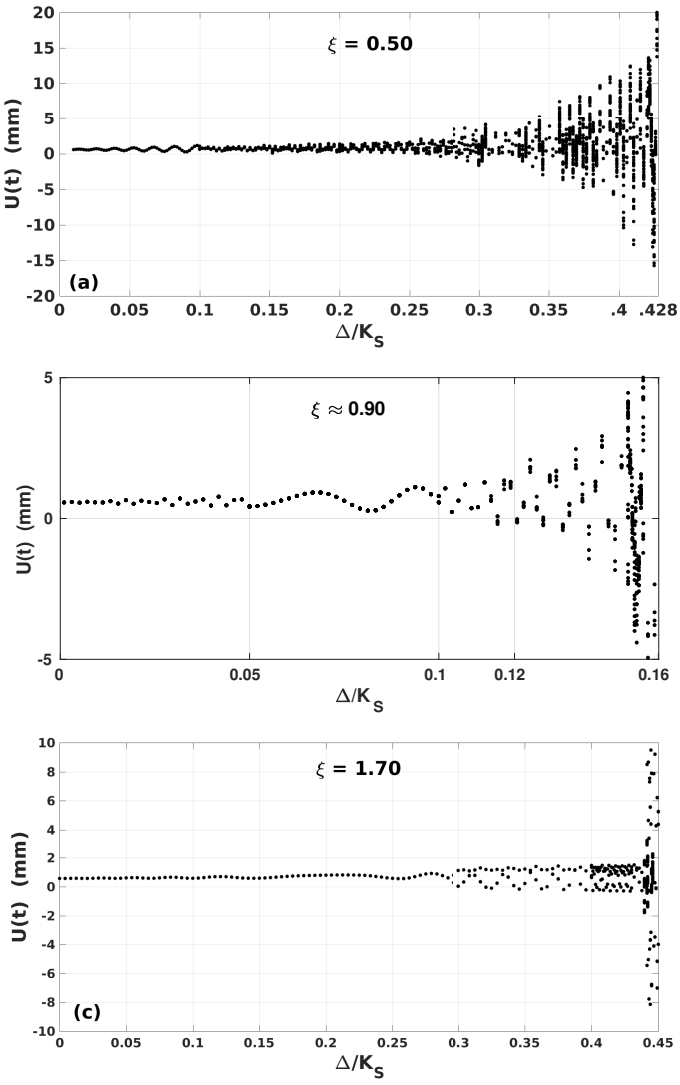

Fig. 12 *Bifurcation diagram (Poincaré section). $d = 3\%$.*

one corresponds to subcritical excitation frequencies (around $\xi < 0.70$). The second one is located around the exact resonance ($\xi \approx 1$). The third zone is located at super-critical rotating speeds close to $\xi \approx 2$.

Contrary to the model of Gasch [14] which does not foresee instabilities for $\xi > 2$, the current model shows a large zone of instability for this speed range. This zone which disappears for high dissipation values, cf. Fig.11(c), has been also noticed by El Arem and Maitournam [12] in the study of the vibrations of a cracked shaft using

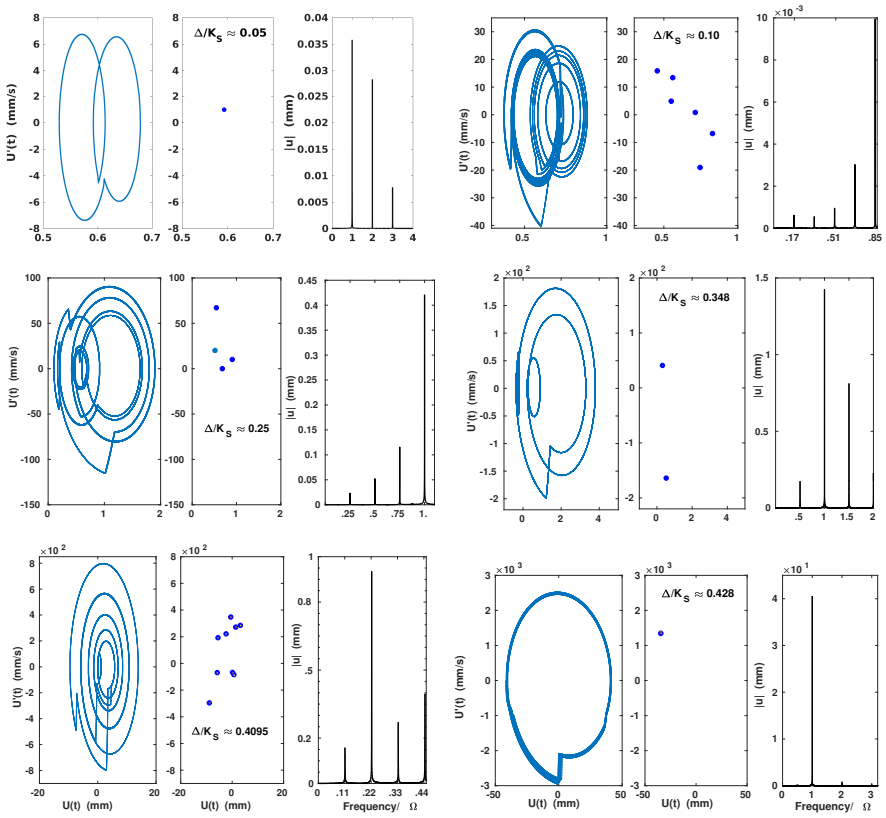

Fig. 13 *Shaft response: phase diagram, Poincaré section, amplitude spectra,* $\xi = 0.50$*,* $d = 3\%$

a new finite element with a stiffness variation identified based on 3D finite element computations. However, real shafts are often exploited at $\xi < 3$, thus we don't focus on the instability zone for $\xi > 3$.
For the bifurcation analysis, it is important that the considered data corresponds to a fully stabilized shaft motion. Hence, the first 3 000 rotations have been discarded in all cases. For the amplitude spectra plots, data of more than 5 000 rotations is considered.
Fig.12 shows the bifurcation diagrams for three different rotating frequencies. It appears that the system response remains bounded for sub- and supercritical forcing frequencies even after the loss of stability of the periodic solution. However, this stability loss could lead to different routes to chaos.

For $\xi = 0.50$, the vibratory response becomes unbounded only at $\frac{\Delta}{K_s} > 0.428$ which corresponds to a very high value of lost stiffness that could not be reached for real machines before the shaft collapse, cf. Fig.12(a). This response remains period one $(1XT = \frac{1}{\Omega})$ till $\frac{\Delta}{K_s} \approx 0.074$ (superharmonic resonance), then the period starts

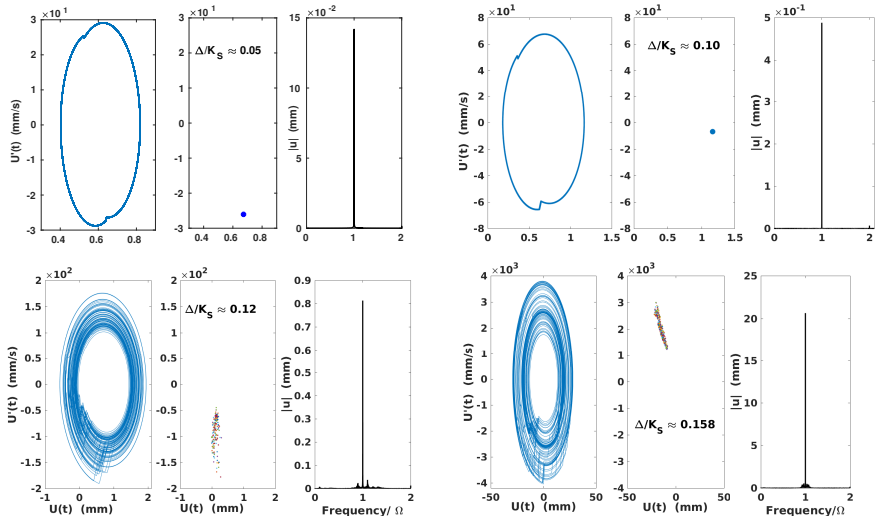

Fig. 14 *Shaft response: phase diagram, Poincaré section, amplitude spectra,* $\xi = 0.90$*,* $d = 3\%$

changing continuously with the crack depth increasing. It changes to $6T$ at $\frac{\Delta}{K_s} \approx 0.10$, $4T$ at $\frac{\Delta}{K_s} \approx 0.25$, $2T$ at $\frac{\Delta}{K_s} \approx 0.348$ and $9T$ at $\frac{\Delta}{K_s} \approx 0.4095$. At the limit of this bounded response ($\frac{\Delta}{K_s} \approx 0.428$), the system rotation is period one again before entering the chaotic zone where it becomes unbounded. The phase diagram, Poincaré section and amplitude spectra plotted for different crack depths confirm this period change preceding the chaotic zone entrance, cf. Fig.13.

According to Fig.14, at $\xi \approx 0.90$, the system response remains periodic of period one till $\frac{\Delta}{K_s} \approx 0.114$ where it enters the hatched zone, cf. Fig.11(b). Thereafter, As it could be depicted from Fig.14, the vibratory response becomes chaotic then unbounded at $\frac{\Delta}{K_s} \approx 0.159$, cf. Fig.12(b).

At $\xi \approx 1.70$, the system oscillations remain periodic of period $T = \frac{1}{\Omega}$ till $\frac{\Delta}{K_s} \approx 0.30$ where a sub-harmonic resonance is observed: the vibratory response goes from period one to period two response, cf. Fig.15. In fact, at the bifurcation point, one of the Floquet's matrix eigenvalues leaves the unit circle through -1. This stable periodic motion persists until $\frac{\Delta}{K_s} \approx 0.439$, afterward the response becomes period three till $\frac{\Delta}{K_s} \approx 0.4501$. For cracks such as $\frac{\Delta}{K_s} > 0.4501$, the response is unbounded, cf. Fig.12(c).

At $\frac{\Delta}{K_s} \approx 0.10$, the obtained solution is period six for $\xi = 0.50$, and period one for $\xi = 0.9$ and 1.70. Changes in the oscillations periodicity when varying the cracked shaft speed has also been noticed in [27].
It is obvious to notice, given this results, that a stable shaft rotating at $\xi \approx 1.70$ could

collapse when slowing down to stop the machine for example since the speed will go through critical values ($\xi \approx 0.90$). The same shaft stable at subcritical rotating frequencies will also collapse while speeding up if its lost stiffness is that $\frac{\Delta}{K_S} > 0.158$. Consequently, for cracked shafts, the passage near the exact resonance ($\xi \approx 1$) should be made with a very selective attention to avoid the machine collapse.
In their exploration of the influence of the crack model on the nonlinear dynamics of a cracked shaft, it was found [27, 13] that in the subcritical speed range, chaotic, quasi-periodic and sub-harmonic responses are completely absent when considering a breathing crack model. These phenomena have been noticed only with a switching crack model and might be due to the instantaneous stiffness change when the crack opens and closes.

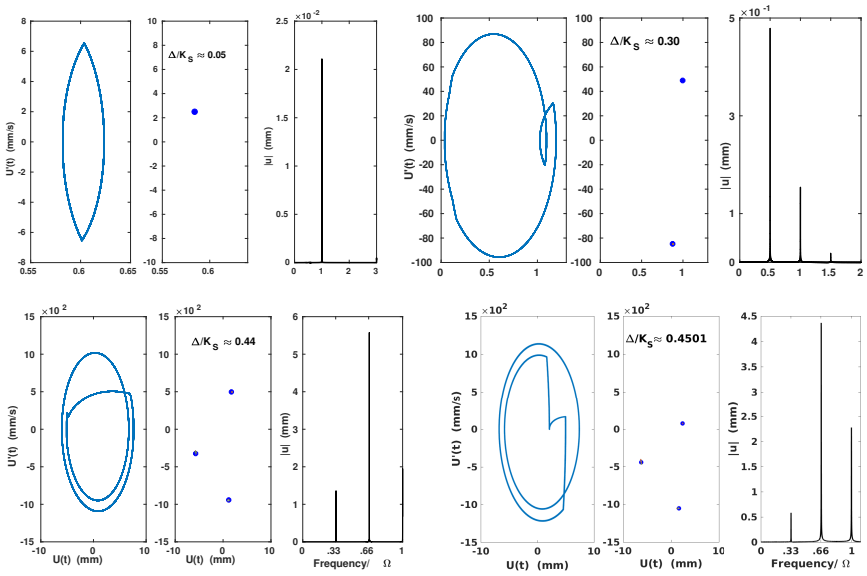

Fig. 15 *Shaft response: phase diagram, Poincaré section, amplitude spectra,* $\xi = 1.70$*,* $d = 3\%$

5 Conclusions

The problem of cracked rotating shafts is very interesting to scientists and engineers working in sectors like aeronautics, aerospace, and power generation. In this article, we have considered a simple and very comprehensive mechanical system to highlight the crack breathing mechanism effects on the system vibratory response. The mechanical system is composed of two non-cracked rigid bars connected with a nonlinear bending spring that concentrates the global stiffness of the cracked shaft. The switching crack model is adopted to describe the breathing mechanism of the crack

and presented as a specific case of the EDF-LMS family of models. By focusing mainly on this mechanism which is at the origin of the nonlinear aspect of the problem, the equilibrium equations are written in a simple, comprehensive and uncluttered form. When the simplifying assumption of weight-governed oscillations is utilized, the breathing mechanism becomes dependent only on the angular position of the crack Ωt leading to linear equilibrium equations that we have solved by means of the harmonic balance method. In particular, we showed that with a switching crack model, the abrupt opening/closing of the crack generates shocks with velocity jumps visible on the shaft phase portrait and responsible for coupling between the system transverse oscillations. We have found, as well-established in the literature, that the breathing crack induces higher harmonics in the vibratory response of the cracked shaft. For supercritical rotating frequencies, the increase of the static deflection and the vibratory amplitude could be used for early detection of propagating cracks. Also, using the Floquet's theory, we have carried out the stability analysis of the shaft with propagating crack and at a reasonable range of rotating frequencies. We have clearly identified three zones of instabilities that correspond to three distinct routes to chaos. It is important to notice that the vibratory response of the system remains bounded for both subcritical and supercritical speeds even for deep cracks and that the most dangerous speed range is close to the first critical speed ($\xi \approx 1.0$). Also we have noticed chaotic response which is completely absent when considering a smoothly breathing crack instead of a switching crack model like in this article. We can confidently attribute these observations to the instantaneous change in the system stiffness when the crack breathes.

Conflict of Interest: The author declare that he has no conflict of interest

References

1. Al-Shudeifat MA, Butcher EA (2011) New breathing functions for the transverse breathing crack of the cracked rotor system: Approach for critical and subcritical harmonic analysis. Journal of Sound and Vibration 330(3):526 – 544
2. Andrieux S, Varé C (2002) A 3d cracked beam model with unilateral contact-application to rotors. European Journal of Mechanics, A/Solids 21:793–810
3. Bachschmid N, Pennacchi P, Tanzi E (2009) Cracked Rotors: A Survey on Static and Dynamic Behaviour Including Modelling and Diagnosis. Springer
4. Bui HD (1978) Mécanique de la rupture fragile (in french). Masson
5. Darpe AK, Gupta K, , Chawla A (2004) Coupled bending, longitudinal and torsional vibrations of a cracked rotor. J Sound Vib 269:33–60
6. Dimarogonas AD (1996) Vibration of cracked structures: A state of the art review. Engineering Fracture Mechanics 55(5):831–857
7. Dimarogonas AD, Paipetis SA, Chondros TG (2013) Analytical Methods in Rotor Dynamics: Second Edition. Springer Netherlands
8. El Arem S (2006) Vibrations non-lineaires des structures fissurées: application aux rotors de turbines (in french). PhD thesis, Ecole Nationale des Ponts et Chaussées

9. El Arem S (2009) Shearing effects on the breathing mechanism of a cracked beam section in bi-axial flexure. European Journal of Mechanics, A/Solids 28:1079–1087
10. El Arem S, Ben Zid M (2017) On a systematic approach for cracked rotating shaft study: breathing mechanism, dynamics and instability. Nonlinear Dynamics 88:2123–2138
11. El Arem S, Maitournam H (2007) Un élément fini de poutre fissurée: application à la dynamique des arbres tournants (in french). European Journal of Computational Mechanics 16(5):643–663
12. El Arem S, Maitournam H (2008) A cracked beam finite element for rotating shaft dynamics and stability analysis. Journal of Mechanics of Materials and Structures 3(5):893–910
13. El Arem S, Nguyen QS (2012) Nonlinear dynamics of a rotating shaft with a breathing crack. Annals of Solid and Structural Mechanics 3(1):1–14
14. Gasch R (1993) A survey of the dynamic behavior of a simple rotating shaft with a transverse crack. J Sound and vibration 160:313–332
15. Géradin M, Rixen D (1997) Mechanical vibrations: Theory and application to structural dynamics. John Wiley & Sons, Second Edition
16. Guo C, Yan J, Yang W (2017) Crack detection for a jeffcott rotor with a transverse crack: An experimental investigation. Mechanical Systems and Signal Processing 83:260 – 271
17. Irwin GR (1957) Analysis of stresses and strains near the end of a crack traversing a plate. J App Mech 24:361–364
18. Ishida Y (2008) Cracked rotors: Industrial machine case histories and nonlinear effects shown by simple jeffcott rotor. Mechanical Systems and Signal Processing 22:805–817
19. Jun OS, Eun HJ, Earmme Y, Lee C (1992) Modelling and vibration analysis of a simple rotor with a breathing crack. J Sound and Vibration 155(2):273–290
20. Khorrami H, Rakheja S, Sedaghati R (2017) Vibration behavior of a two-crack shaft in a rotor disc-bearing system. Mechanism and Machine Theory 113:67 – 84
21. Mayes I, DAVIES W (1984) Analysis of the response of a multi-rotor-bearing system containig a transverse crack in a rotor. J Vib Acous Stress Reliab Design 106:139–145
22. Meng G, Gasch R (2000) Stability ans stability degree of a cracked flexible rotor supported on journal bearings. J Vibration and Acoustics, Transactions of ASME 122:116–125
23. Muller P, Bajkowski J, Soffker D (1994) Chaotic motions and fault detection in a cracked rotor. Nonlinear Dynamics 5:233–254
24. Nayfeh AH, Mook DT (1979) Nonlinear oscillations. John Wiley & Sons
25. Papadopoulos C (2004) Some comments on the calculation of the local flexibility of cracked shafts. Journal of Sound and Vibration 278:1205 – 1211
26. Papadopoulos CA (2008) The strain energy release approach for modeling cracks in rotors: A state of the art review. Mechanical Systems and Signal Processing 22(4):763 – 789

27. Patel TH, Darpe AK (2008) Influence of crack breathing model on nonlinear dynamics of a cracked rotor. J Sound and Vibration 311:953–972
28. Sinou JJ (2009) Experimental response and vibrational characteristics of a slotted rotor. Communications in Nonlinear Science and Numerical Simulation 14(7):3179 – 3194
29. Sinou JJ (2009) Experimental study on the nonlinear vibrations and nx amplitudes of a rotor with a transverse crack. Journal of Vibration and Acoustics 131(4):1–6
30. Stoisser C, Audebert S (2008) A comprehensive theoretical, numerical and experimental approach for crack detection in power plant rotating machinery. Mechanical Systems and Signal Processing 22(4):818–844
31. Wauer J (1990) On the dynamics of cracked rotors: A literature survey. Applied Mechanical Reviews 43(1):13–17
32. Zhou T, Sun Z, Xu J, Han W (2004) Experimental analysis of cracked rotor. Journal of Dynamic Systems, Measurement, and Control 127(3):313–320